Superconductivity in two-dimensional boron allotropes

Yinchang Zhao, Shuming Zeng, and Jun Ni*

State Key Laboratory of Low-Dimensional Quantum Physics, Department of Physics, Tsinghua University, Beijing 100084, People's Republic of China and Collaborative Innovation Center of Quantum Matter, Beijing 100084, People's Republic of China

(Received 12 October 2015; revised manuscript received 25 November 2015; published 6 January 2016)

We use *ab initio* evolutionary algorithm and first-principles calculations to investigate structural, electronic, vibrational, and superconducting properties of two-dimensional (2D) boron allotropes. Remarkably, we show that conventional BCS superconductivity in the stable 2D boron structures is ubiquitous with the critical temperature T_c above the liquid hydrogen temperature for certain configurations. Due to the electronic states of the Fermi surface originating from both σ and π electrons, the superconductivity of the 2D structures arises from multiple phonon modes. Our results support that 2D boron structure may be a pure single-element material with the highest T_c on conditions without high pressure and external strain.

DOI: 10.1103/PhysRevB.93.014502

I. INTRODUCTION

According to conventional BCS theory [1], metals composed of light elements are beneficial for increasing the superconducting transition temperature (T_c), because the Debye temperatures of these metals are typically high. Generally, these materials require high pressure to produce superconducting phase. For instance, dense molecular hydrogen under superhigh pressure (450 GPa) is predicted to have the highest T_c of 242 K [2–4]; the light metallic element Li under the pressure of about 40 GPa shows a $T_c \approx 70$ K [5,6]; and the recent reported binary compound hydrogen sulfide shows a T_c of 190 K under pressure higher than 200 GPa [7]. In these materials, high pressure leads to structural phase transition, and consequently change of electronic and superconducting properties. For example, in hydrogen sulfide the H_3S structural phase is produced under pressure of 200–250 GPa, which gives a strong electron-phonon coupling (EPC) ($\lambda \sim 1.84$ at 200 GPa) [8]. However, of these materials, most of the compounds containing boron, such as MgB_2 and its analogs, superconduct under ambient pressure [9–20], in spite of the Mg-doped β-rhombohedral boron structure lacking superconductivity [21]. In the binary compound MgB_2, superconductivity stems from the graphitelike boron layers, due to the in-plane stretching vibrational modes of boron bonds showing a strong coupling with the self-doped charge carriers from magnesium to boron [10–14]. Enlightened by the boron driven superconductivity in MgB_2 and considerable T_c in light single-element materials, here we focus on the superconducting properties of pure boron material. To date no evidence of superconductivity in the pure boron under ambient pressure has been reported, although a superconducting phase with $T_c \sim 11$ K is proposed in bulk boron under the pressure of 250 GPa [22,23]. However, for low-dimensional structures, Be has a T_c of 10.5 K in thin films [24], one-atomic-layer Pt film grown on Si(111) is a superconductor [25], and graphene has a T_c of 30 K under 16% strain combined with 4×10^{14} cm^{-2} carriers doping [26]. Therefore, we turn to the two-dimensional (2D) boron structures to search superconducting phase in boron under ambient pressure.

For 2D boron structures, because of structural and chemical complexity, stabilities and electronic properties have been studied extensively [27–39]. First of all, a triangular arranged lattice with buckling was once thought to be a stable boron sheet and used to construct boron nanotubes [27]. Then the boron sheets formed from both triangular and hexagonal motifs, represented by the so-called α-sheet structure, are proposed to be energetically most stable [28,29]. Recently, a new type of 2D boron configuration with a symmetric group of $Pmmn$, which shows an electronic property of massless dirac fermions, has been predicted to be more stable than the α sheet [38]. But the superconductivity in this 2D material has not been studied until now. In this paper, we concentrate on the electronic, vibrational, and superconducting properties in 2D boron structures, and conclude that superconductivity in the stable 2D boron structures is ubiquitous, at least in the structures considered. Our results support that a 2D boron structure may be a pure single-element material with the highest T_c on conditions without high pressure and external strain. Calculation details are described in Sec. II. The results on electronic and superconducting properties of all 2D boron structures considered are presented in Sec. III. Section IV is our summary.

II. METHODOLOGY

To gain stable structural phases, we employ the *ab initio* evolutionary algorithm USPEX [40–42] combined with the first-principles code VASP5.3.3 [43,44] to search the 2D boron allotropes. The initial structures are randomly generated according to the plane group symmetry with a given initial thickness. We focus on using the monolayer, bilayer, and thin multilayer 2D boron structures to study superconductivity, and thus select the thickness values of 3.2, 4.6, and 6.0Å to do three times searches based on the experimental value of spacing (3.2Å) between two adjacent layers of multiwalled boron nanotubes [45]. In these calculations, the structural optimization of all the newly generated structures are carried out by VASP due to its high efficiency to relax structures [43,44]. After stable structural phases are searched, corresponding electronic properties are calculated by the VASP. A cutoff energy of 500 eV is used with the exchange-correlation functional of generalized gradient approximation (GGA) of

*junni@mail.tsinghua.edu.cn

Perdew-Burke-Ernzerhof (PBE) [46]. The Monkhorst-Pack sampling grid with a resolution of $2\pi \times 0.01\text{Å}^{-1}$ is used to simulate the k-space integrations. In addition, to test the structural stabilities, we also select the hybrid HSE06 functional [47] to recalculate the structural parameters and total energies of the newly searched structures. To calculate the vibrational and superconducting properties, the QUANTUM-ESPRESSO package [48] is employed in view of its effectiveness to calculate the phonon and EPC [26,49]. The structural and electronic properties are recalculated by QUANTUM-ESPRESSO, and consistent results with those calculated by VASP are obtained. The ultrasoft pseudopotential with a cutoff energy of 55 Ry is utilized, which is sufficient to converge the EPC parameter and T_c (see Fig. 1 in Ref. [50]). Phonon frequencies are calculated based on the linear-response technique on the phonon wave-vector mesh with the resolution of $2\pi \times 0.02\text{Å}^{-1}$ and corresponding uniform electron-momentum grid with the resolution of $2\pi \times 0.01\text{Å}^{-1}$. For calculations of the EPC parameter, a denser electron momentum k mesh with a resolution of $2\pi \times 0.005\text{Å}^{-1}$ is used. The resolutions for phonon wave-vector mesh and electron-momentum grid are higher than those in previous work which calculated superconductivity by the same method as ours [49], guaranteeing the convergence of q mesh and k mesh in all of our calculations.

III. RESULTS AND DISCUSSION

There are many low-energy structures produced by USPEX. We only pay attention to the energetically stable structures with high symmetry in each search, because of the low-symmetry configurations implying the frustration of the 2D system. These structures are mainly found in the searches with six, eight, and ten atoms per unit cell. For the typical instance (eight-atom system, which represents there are eight atoms per unit cell, similar to the α-sheet structure), three stable structures are found, as shown in Fig. 1. Based on their symmetric groups and atom numbers, they are designated as 8-$Pmmm$ and 8-$C2/m$ boron structures. There are two different structures belonging to the same symmetric group of $C2/m$. We label them as 8-$C2/m$-I boron and 8-$C2/m$-II boron, as shown in Figs. 1(c) and 1(d), respectively. The 8-$Pmmm$ boron is made of two buckled triangular layers, as shown in Fig. 1(b), and consequently the 8-$C2/m$-I and 8-$C2/m$-II boron structures can be taken as stacking of four hexagonal layers with the stacking pattern of ABAB and ABCD, respectively. For the six-atom and ten-atom systems the most stable structures have the symmetric group of $C2/m$ (named as 6-$C2/m$) and Cm (named as 10-Cm), respectively, which resemble the 8-$C2/m$ boron structures but possess different stacking patterns (see Fig. 2 in Ref. [50]). Due to forming from multihexagonal layers, the 6-$C2/m$, 8-$C2/m$, and Cm structures can be taken as thin multilayers. In fact, theses structures are all made up of the triangular motifs, as shown in Fig. 1, which is in accordance with the boron Aufbau principle that the most stable structures are composed of the triangular motifs [27]. For detailed structural parameters, see Tables I and II in Ref. [50].

Considering ambient pressure has almost no contribution to enthalpy (the order of magnitude of PV is 10^{-4} eV), we

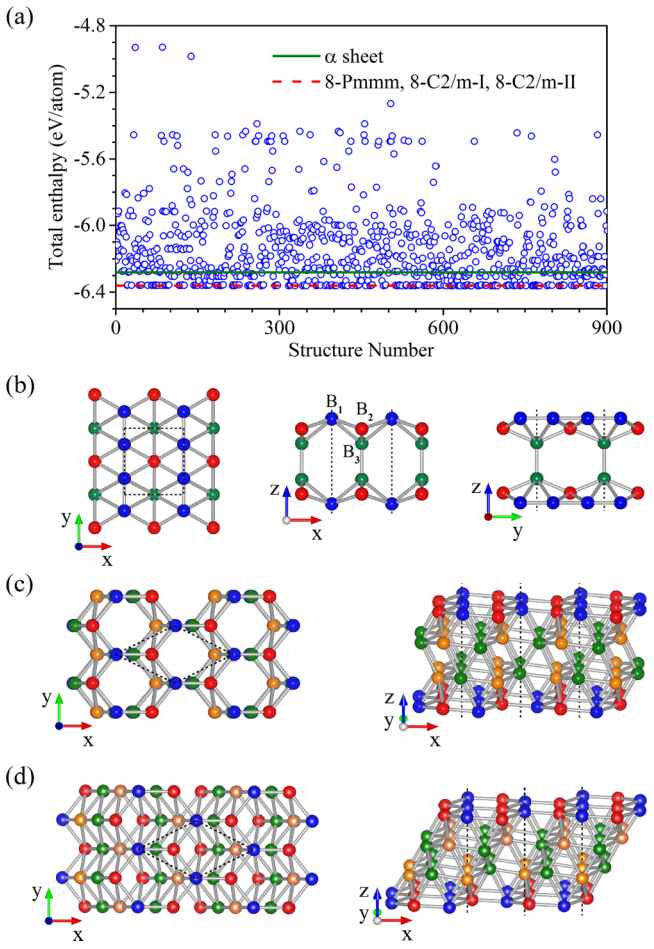

FIG. 1. (a) A typical instance of enthalpy evolution for the eight-atom system. Three stable structures are produced after the evolution. Top and lateral views of the structures are shown in (b) (8-$Pmmm$), (c) (8-$C2/m$-I), and (d) (8-$C2/m$-II), respectively. Atoms with different color are nonequivalent. In (b) three kinds of nonequivalent atoms are also labeled as B_1, B_2, and B_3.

TABLE I. Atom numbers (AN), symmetric groups (SG), formation energies (E_f), and thicknesses of the newly searched boron structures. For the formation energies and thicknesses the results estimated from GGA-PBE and HSE06 functionals are both shown. For comparison, values for monolayer buckled triangular boron (MBT) and α-bulk boron are also listed.

	AN	SG	E_f (eV/atom)		Thickness (Å)	
Phase			PBE	HSE06	PBE	HSE06
MBT	2	$Pmmn$	5.75	5.59	0.88	0.90
α sheet	8	$P\bar{3}m1$	5.87	5.71	0.34	0.40
6-$C2/m$	6	$C2/m$	6.03	5.80	3.06	3.05
8-$Pmmm$	8	$Pmmm$	6.05	5.81	4.09	4.10
8-$C2/m$-I	8	$C2/m$	6.05	5.81	4.78	4.78
8-$C2/m$-II	8	$C2/m$	6.05	5.82	4.53	4.50
10-Cm	10	$C2/m$	6.07	5.83	6.26	6.20
α bulk	12	$R\bar{3}m$	6.26	6.18		

TABLE II. Calculated values of N_F, V_{ep}, λ, $\omega_{\log}$, and T_c for MgB_2, α sheet, 6-$C2/m$, 8-$Pmmm$, 8-$C2/m$-I, 8-$C2/m$-II, 10-Cm, and monolayer buckled triangular boron (MBT). T_c is calculated by the McMillan-Allen-Dynes formula [52] with $\mu^* = 0.05$.

	N_F (S/(eV cell))	V_{ep} (eV)	λ	$\omega_{\log}$ (cm^{-1})	$T_c^{\mu^*=0.05}$ (K)
MgB_2	0.71	1.04	0.74	722.7	39.9
α sheet	0.86	0.60	0.52	262.2	6.7
6-$C2/m$	0.81	0.52	0.42	636.6	8.5
8-$Pmmm$	1.08	0.56	0.60	500.8	18.2
8-$C2/m$-I	1.08	0.34	0.37	666.2	5.7
8-$C2/m$-II	1.07	0.67	0.72	525.3	27.6
10-Cm	1.29	0.45	0.58	572.6	18.9
MBT	0.38	2.26	0.86	364.3	25.6

use the formation energy $E_f = (E_s - E_t)/n$ to see structural stabilities of the newly searched 2D boron structures, where n is the number of atoms in each primitive cell, and E_t (E_s) the total energy of the 2D boron structure (isolated boron atom). The formation energies together with the atom numbers, thicknesses, and symmetric groups of the 2D boron structures are listed in Table I. For comparison, values for the α-bulk boron and monolayer buckled triangular boron are also listed. The E_f (total energy) of the α-bulk boron calculated from the GGA-PBE functional is 6.26 (−6.68) eV/atom, which is consistent with the previous work [51]. Obviously, the newfound structures are more stable than the α sheet, but are less stable than the α-bulk boron, indicating that the new 2D phases are metastable (as expected for any 2D structure). Furthermore, both GGA-PBE and HSE06 calculations approximately show that the structure with the larger thickness has the higher formation energy, complying with the rule that the formation energy increases as the system transitions from a 2D structure to a 3D structure. For the eight-atom system, three stable structures have the same structural stability as the GGA-PBE calculations, although the HSE06 results show that the E_f of the 8-$C2/m$-II boron is slightly larger than that of the 8-$Pmmm$ and 8-$C2/m$-I structures. In addition, if the initial thicknesses in USPEX are increased step by step there are infinitely many stable structures. Considering computational cost, we focus on the 2D boron structures listed in Table I.

Within BCS theory [1], T_c depends on the effective pairing attractive potential V_{ep}, characteristic phonon frequency ω_0, and electronic density of states (EDOS) N_F at the Fermi level E_F. The EPC parameter λ is equal to $N_F V_{ep}$. The refined expression of T_c is the McMillan-Allen-Dynes formula [52]. In calculations of T_c, the retarded Coulomb pseudopotential μ^* in the McMillan-Allen-Dynes formula is adjustable [52]. To estimate μ^*, we calculate the T_c for MgB_2 (see Fig. 3 in Ref. [50]). If $\mu^* = 0.05$, the T_c of 39.9 K with a λ of 0.74 is obtained, which is consistent with the experimental T_c of 40 K with $\lambda_{exp} \sim 0.75$ [53]. Therefore, we use the μ^* of 0.05 in our estimations for T_c of the 2D boron structures. For the eight-atom system, the 8-$Pmmm$ and 8-$C2/m$-II structures have the T_c of 18.2 K and 27.6 K with $\lambda \sim 0.60$ and 0.72, respectively, as listed in Table II. However, the T_c (5.7 K) of the 8-$C2/m$-I boron is relatively lower, although the N_F of the 8-$C2/m$-I boron almost equals that of the 8-$Pmmm$ or 8-$C2/m$-II structure. For the 6-$C2/m$ and 10-Cm structures, the T_c's of 8.5 and 18.9 K are obtained, respectively. To reveal the superconducting mechanism in these 2D structures, we first concentrate on the bilayer structure (8-$Pmmm$ boron), then the thin multilayer structures (e.g., 8-$C2/m$ boron), and finally the α-sheet (as a representative of the monolayer sheets).

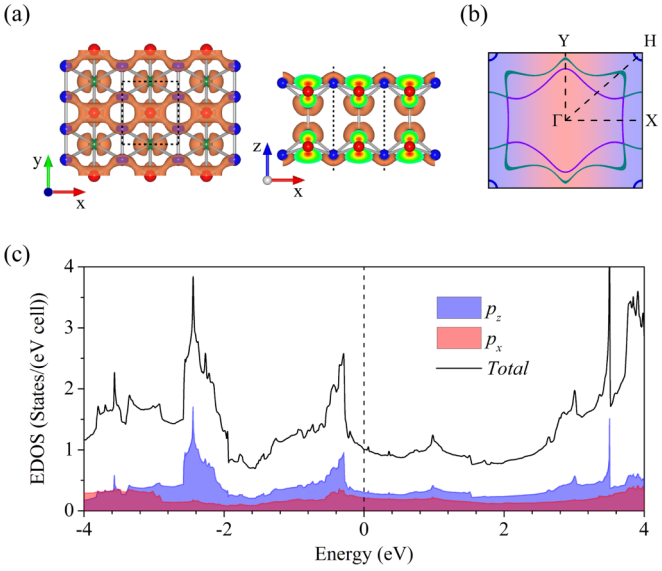

FIG. 2. Electronic structure for the 8-$Pmmm$ boron. (a) Charge distribution of FS electrons. The hybridized feature of the p_x and p_z orbitals is shown. (b) FS. The violet, dark-cyan, and dark-blue lines represent three bands crossing the E_F. The bands in the red section of the BZ show p_x character, while those in the blue section have p_z character. (c) Projected EDOS. The red and blue colors represent the p_x and p_z orbitals, respectively.

For the bilayer structure 8-$Pmmm$ boron, we show the Fermi surface (FS), projected EDOS, and charge distribution of states of FS in Fig. 2. There are three energy bands crossing the FS, as shown in Fig. 2(b). Projected EDOS shows that the hybridized states between the p_x and p_z orbitals form the FS, giving rise to a $N_F \sim 1.08$ states/(eV cell), as shown in Fig. 2(c). More precisely, the p_x (p_z) electrons mainly arise from the B_1 and B_3 (B_2) atoms labeled in Fig. 1(b). The charge distribution at E_F further demonstrates the feature of hybrid electronic states of the p_x and p_z electrons, showing characters of both σ and π bonds, as shown in Fig. 1(a). In the Brillouin zone (BZ), the p_z electrons of FS tend to distribute in the region near the vertical BZ boundary (the HX line) while the p_x electrons distribute in the rest region [see Fig. 2(b)]. In addition, almost all of the bonding states of the s and p_y orbitals are occupied, which form the skeleton of the 8-$Pmmm$ structure (see Fig. 4 in Ref. [50]).

In Fig. 3(a) we plot the phonon dispersion with phonon linewidth, phonon density of states (PDOS), and Eliashberg function for the 8-$Pmmm$ boron. The Eliashberg function, which shows the relative contribution of different modes to EPC parameter λ, is defined as

$$\alpha^2 F(\omega) = \frac{1}{2\pi N_F} \Sigma_{\mathbf{q}\nu} \delta(\omega - \omega_{\mathbf{q}\nu}) \frac{\gamma_{\mathbf{q}\nu}}{\hbar \omega_{\mathbf{q}\nu}}, \quad (1)$$

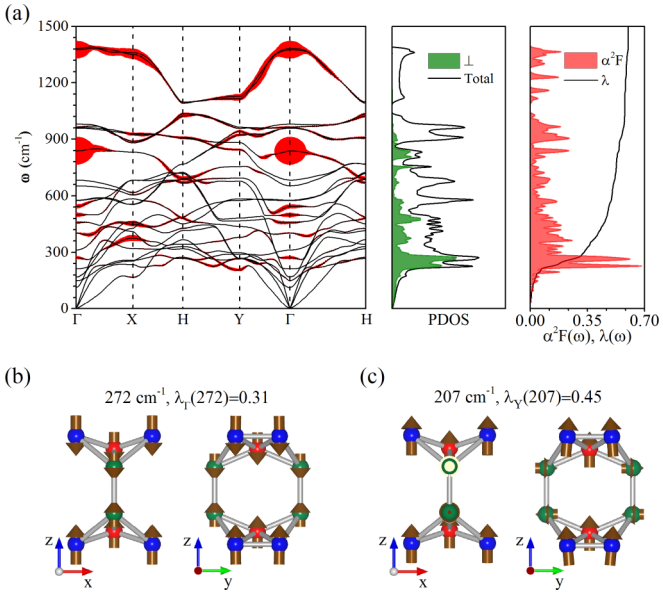

FIG. 3. Vibrational and superconducting properties for the 8-$Pmmm$ boron. (a) Phonon dispersion with phonon linewidth $\gamma_{\mathbf{q}\nu}$, total PDOS with out-of-plane projected PDOS, and Eliashberg function $\alpha^2F(\omega)$ with $\lambda(\omega)$. (b) A_g mode at the Γ point ($\omega = 272$ cm^{-1}). (c) B_{3g} mode at the Y point ($\omega = 207$ cm^{-1}).

where $\gamma_{\mathbf{q}\nu}$ is the phonon linewidth of the mode ν with momentum $\mathbf{q}$, which is calculated by

$$\gamma_{\mathbf{q}\nu} = 2\pi\omega_{\mathbf{q}\nu}\Sigma_{i,j}\int\frac{d^3k}{\Omega_{BZ}}|g_{\mathbf{q}\nu}(\mathbf{k},i,j)|^2\delta(e_{\mathbf{q},i}-e_F) \times\delta(e_{\mathbf{k}+\mathbf{q},i}-e_F), \quad (2)$$

where $\omega_{\mathbf{q}\nu}$ are the phonon frequencies, and $g_{\mathbf{q}\nu}(\mathbf{k},i,j) = (\hbar/2M\omega_{\mathbf{q}\nu})^{1/2}\langle\psi_{i,\mathbf{k}}|dV_{SCF}/d\mathbf{u}_{\mathbf{q}\nu}|\psi_{j,\mathbf{k}+\mathbf{q}}\rangle$ is the electron-phonon matrix element. Phonon dispersion and projected PDOS show that in low-frequency range (0–340 cm^{-1}) there are mainly out-of-plane modes arising from the B_1 atoms and in-plane modes originated from the B_1 and B_3 atoms. Among them the out-of-plane modes occupy about 65% of the total PDOS in this frequency range, as shown in Fig. 3(a). For detailed projected PDOS, see Fig. 1 in Ref. [50]. The softest acoustic modes around the high symmetry line HY give rise to the first peak of PDOS, while the accompanying phonon linewidth causes the maximum peak of the Eliashberg function. Similarly, the out-of-plane soft optical modes contribute to forming the second peak of PDOS, and the corresponding phonon linewidth leads to the second maximum peak of the Eliashberg function, as shown in Fig. 3(a). These low-frequency modes polarize just the FS electrons with the p_z and p_x characters, facilitating the formation of Cooper pairs, and consequently result in a λ of 0.36. To see these vibration modes clearly, the softest acoustic mode at the Y point (B_{3g} mode with $\omega \sim 207$ cm^{-1}), a typical softest mode around high-symmetry line HY, is shown in Fig. 3(c), which induces about a half of the total EPC at the Y point. The A_g mode at the Γ point with $\omega \sim 272$ cm^{-1}, a typical instance of the out-of-plane soft optical modes, is shown in Fig. 3(b), which contributes about one-third of the total EPC at the Γ point. Because of strong EPC, the response of the FS electrons to the modes shown in Figs. 3(b) and 3(c) is obviously drastic (see Fig. 6 in Ref. [50]). In the intermediate frequency range (340–1000 cm^{-1}), 75% of vibrations are the in-plane optical modes, while the rest are the out-of-plane modes. Furthermore, 80% of the in-plane modes vibrate along the x direction. These vibration modes are more favorable to the polarization of the p_x electrons in FS and consequently contribute to a λ of 0.22. For high frequency (above 1000 cm^{-1}), there are only the in-plane modes of the B_1 atoms, which correspond to the stretching modes of the y-directional σ bonds. These modes have weak coupling with the FS electrons, and consequently generate a small λ of 0.02. As a result, the total λ of 0.60 is gained, about 50% of which stems from the in-plane modes. Using $N_F \sim 1.08$ states/(eV cell) and $\lambda = N_F V_{ep}$, the pairing attractive potential $V_{ep} \sim 0.56$ eV is obtained, which is about a half of that in MgB_2, as listed in Table II. In addition, to reveal the relations between structural and superconducting properties, we also calculate the electronic and superconducting properties of the buckled triangular monolayer. Because the buckled triangular monolayer is the parent material of the 8-$Pmmm$ boron, the FS electrons of the monolayer also consist of the p_x and p_z orbitals (see Fig. 7 in Ref. [50]). But a stronger EPC ($\lambda \sim 0.86$) with a much larger V_{ep} (~2.26 eV) than that of the 8-$Pmmm$ boron is gained in the monolayer, as listed in Table II. This is due to the fact that the out-of-plane modes of 8-$Pmmm$ boron are partly suppressed by its bilayer structure, which results in a weaker pairing attractive potential and EPC than those in the monolayer. For the vibrational and superconducting properties of the buckled triangular monolayer, see Fig. 8 in Ref. [50].

Since the 8-$C2/m$-I and 8-$C2/m$-II structures have the same atom numbers as the 8-$Pmmm$ boron, we use the 8-$C2/m$-I and 8-$C2/m$-II structures to reveal the implicit superconducting mechanism for thin multilayers. The electronic structures of the 8-$C2/m$-I and 8-$C2/m$-II boron structures are shown in Fig. 4. In contrast to the 8-$Pmmm$ boron, there are two energy bands crossing the FS, as shown in Figs. 4(a) and 4(b). The FS of the 8-$C2/m$ structures are mainly composed of the hybridized states between the p_y and p_z orbitals, as shown by the EDOS plotted in Figs. 4(c) and 4(d). The electrons on FS are apt to distribute in the surface boron layer, where the electron distribution shows the feature of hybrid states of the p_y and p_z electrons in real space [see Figs. 4(a) and 4(b)]. In BZ, the p_y electrons on FS tend to distribute in the central region, while the p_z electrons distribute around the BZ boundary. In addition, almost all of the bonding states of the s and p_x orbitals are occupied, which have negligible contribution to the FS (see Fig. 9 in Ref. [50]).

For the 8-$C2/m$-I structure, when $\omega < 720$ cm^{-1}, the λ mainly arises from the in-plane acoustic modes and out-of-plane optical modes. Within these vibration modes the surface boron atoms possess the maximum amplitudes. This leads to strong EPC between these modes and the p_y and p_z electrons in the surface boron layer, giving rise to a λ of 0.31, as shown in Fig. 5(a). Above 720 cm^{-1}, the x- and z-directional optical vibrations generate a λ of 0.06. Finally, a total λ of 0.37 is gained in this configuration. For the 8-$C2/m$-II boron, the origin of EPC is similar to that of the 8-$C2/m$-I structure, but the out-of-plane acoustic modes (the softest modes) around the BZ boundary are much more strongly

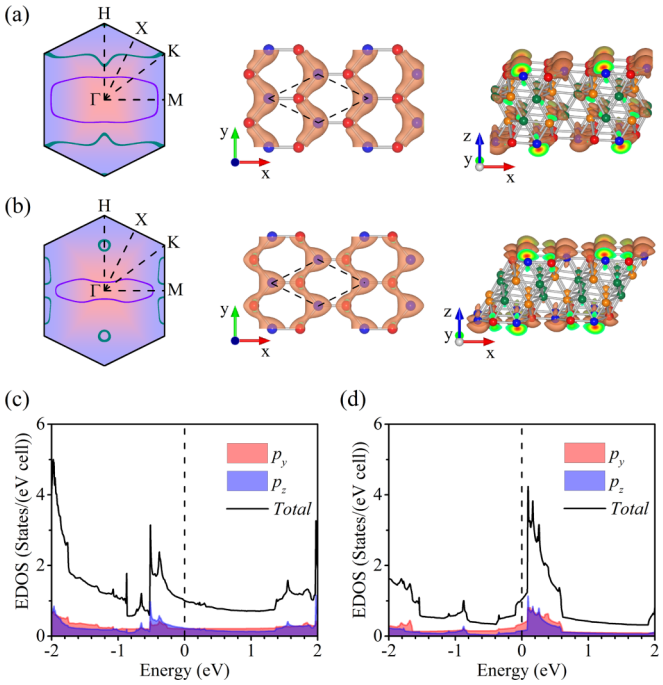

FIG. 4. (a) and (b) show FS and distribution of the FS electrons for 8-$C2/m$-I and 8-$C2/m$-II, respectively. The violet and dark-cyan lines in FS represent two bands crossing the E_F. In charge distribution the hybridized feature of the p_y and p_z orbitals is shown. (c) and (d) plot the projected EDOS for 8-$C2/m$-I and 8-$C2/m$-II, respectively. The red and blue colors represent the p_y and p_z orbitals, respectively.

coupled with the FS electrons, as shown in Fig. 5(b). This leads to an apparent softening of phonon frequencies and correspondingly an additional λ of about 0.33 in comparison

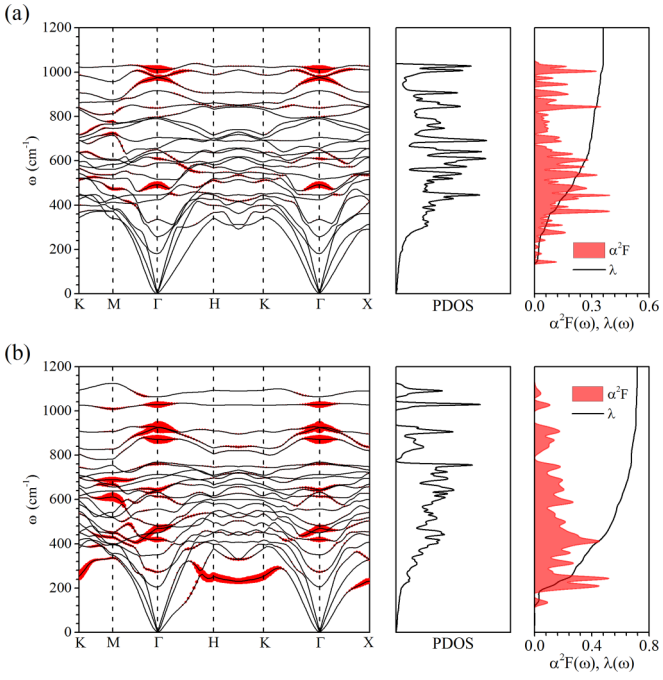

FIG. 5. Phonon dispersion with phonon linewidth $\gamma_{\mathbf{q}\nu}$, total PDOS, and Eliashberg function $\alpha^2F(\omega)$ with $\lambda(\omega)$ for (a) 8-$C2/m$-I boron and (b) 8-$C2/m$-II boron.

with the case of the 8-$C2/m$-I boron. Consequently, a total $\lambda \sim 0.72$ is induced in the 8-$C2/m$-II boron structure, which is almost equal to that in MgB_2. As a result, a T_c (27.6 K) higher than the liquid hydrogen temperature is obtained in this 2D boron structure. Obviously, due to strong EPC induced by the softest modes around the BZ boundary, the response of the FS electrons to these modes is drastic in the 8-$C2/m$-II structure (see Fig.10 in Ref. [50]). This can be explained by the EDOS around E_F. Although the N_F is nearly equal, for the 8-$C2/m$-II structure the EDOS above E_F about 0.3 eV is much larger than that for the 8-$C2/m$-I boron, as shown in Figs. 4(c) and 4(d). Only a weak structural change in the 8-$C2/m$-II boron can make the electrons above E_F enter into FS, and then result in the increasing of N_F and EPC.

In addition, for the 6-$C2/m$ boron, the origin of EPC is almost the same as that of the 8-$C2/m$-I structure [see Fig. 11(a) in Ref. [50]]. However, a stronger V_{ep} makes the λ larger than that of the 8-$C2/m$-I boron, although a smaller N_F is gained. Therefore, a higher T_c (∼8.5 K) than that of the 8-$C2/m$-I boron is obtained in the 6-$C2/m$ boron. For the 10-Cm boron, the mechanism of superconductivity is analogous to that of the 8-$C2/m$-II structure. Also the softest acoustic modes around the BZ boundary are much more strongly coupled with the FS electrons [as shown in Fig. 11(b) in Ref. [50]], which leads to a λ of 0.24. Finally, a total λ of 0.58 with a $T_c \sim 18.9$ K is obtained in the 10-Cm boron.

At last, we calculate the superconductivity in the monolayer sheets. Of the monolayer structures, α sheet has the best energy stability because the bonding states of the σ bonds in this structure are totally occupied, leaving the FS composed of only the π electrons [28]. Our results reveal that the α sheet possesses a buckling of 0.34 (0.40) Å along the normal direction of the sheet from the GGA-PBE (HSE06) calculations, as listed in Table I, which is similar to the result in Ref. [34]. In addition, we also relax the structure using the local density approximation (LDA) for the α sheet, and conclude that it is a plane structure with zero thickness along the normal direction, same as the result in Ref. [28]. The buckled α sheet has the symmetric group of $P\bar{3}m1$, in contrast to $P6/mmm$ symmetry of the plane one. Our analyses reveal that the buckling structure facilitates the increase of the EPC between the out-of-plane vibration modes and π electrons in FS (see Fig. 12 in Ref. [50]). As a result, a T_c of 6.7 K with $\lambda \sim 0.52$ is obtained in the buckled α sheet from GGA results, as listed in Table II. However, because of lacking buckling there is an almost zero T_c obtained in the plane α sheet from the LDA calculations.

IV. CONCLUSION

In summary, we have used an *ab initio* evolutionary algorithm to search structural phases of the 2D boron allotropes. Five energetically stable structures with high symmetry are found. Then we discover that superconductivity in these newly found boron structures is ubiquitous with T_c of all the structures higher than the liquid-helium temperature. Our analysis revealed that the EPC in the newly found structures is induced by the multiple vibration modes, due to the electrons in FS arising from the hybridized states of the σ and π bonds. In particular, the T_c of the 8-$C2/m$-II boron is higher than the liquid-hydrogen temperature. Furthermore, according to HSE06 cal-

culations the 8-$C2/m$-II structure is not only higher in formation energy than α sheet but also more stable than the 8-$Pmmm$ and 8-$C2/m$-II structures. These results support that 2D boron structures may be the single-element material with the highest T_c on conditions without high pressure and external strain.

ACKNOWLEDGMENTS

This research was supported by the National Natural Science Foundation of China under Grant No. 11174171 and 11374175.

[1] J. Bardeen, L. N. Cooper, and J. R. Schrieffer, Phys. Rev. **108**, 1175 (1957).
[2] P. Cudazzo, G. Profeta, A. Sanna, A. Floris, A. Continenza, S. Massidda, and E. K. U. Gross, Phys. Rev. Lett. **100**, 257001 (2008).
[3] P. Cudazzo, G. Profeta, A. Sanna, A. Floris, A. Continenza, S. Massidda, and E. K. U. Gross, Phys. Rev. B **81**, 134505 (2010).
[4] P. Cudazzo, G. Profeta, A. Sanna, A. Floris, A. Continenza, S. Massidda, and E. K. U. Gross, Phys. Rev. B **81**, 134506 (2010).
[5] N. E. Christensen and D. L. Novikov, Phys. Rev. Lett. **86**, 1861 (2001).
[6] J. Neaton and N. Ashcroft, Nature (London) **400**, 141 (1999).
[7] A. P. Drozdov, M. I. Eremets, I. A. Troyan, V. Ksenofontov, and S. I. Shylin, Nature (London) **525**, 73 (2015).
[8] I. Errea, M. Calandra, C. J. Pickard, J. Nelson, R. J. Needs, Y. Li, H. Liu, Y. Zhang, Y. Ma, and F. Mauri, Phys. Rev. Lett. **114**, 157004 (2015).
[9] J. Nagamatsu, N. Nakagawa, T. Muranaka, Y. Zenitani, and J. Akimitsu, Nature (London) **410**, 63 (2001).
[10] J. M. An and W. E. Pickett, Phys. Rev. Lett. **86**, 4366 (2001).
[11] J. Kortus, I. I. Mazin, K. D. Belashchenko, V. P. Antropov, and L. L. Boyer, Phys. Rev. Lett. **86**, 4656 (2001).
[12] T. Yildirim, O. Gülseren, J. W. Lynn, C. M. Brown, T. J. Udovic, Q. Huang, N. Rogado, K. A. Regan, M. A. Hayward, J. S. Slusky, T. He, M. K. Haas, P. Khalifah, K. Inumaru, and R. J. Cava, Phys. Rev. Lett. **87**, 037001 (2001).
[13] J. Akimitsu and T. Muranaka, Physica C (Amsterdam) **388**, 98 (2003).
[14] Y. Kong, O. V. Dolgov, O. Jepsen, and O. K. Andersen, Phys. Rev. B **64**, 020501 (2001).
[15] C. Kawabata, N. Hayashi, and F. Ono, Physica C (Amsterdam) **378**, 220 (2002).
[16] L. Boeri, J. Kortus, and O. K. Andersen, Phys. Rev. Lett. **93**, 237002 (2004).
[17] J. Akimitsu, S. Akutagawa, K. Kawashima, and T. Muranaka, Prog. Theor. Phys. Suppl. **159**, 326 (2005).
[18] K.-W. Lee and W. E. Pickett, Phys. Rev. Lett. **93**, 237003 (2004).
[19] J. Nakamura, M. Matsudaira, J. Haruyama, H. Sugiura, M. Tachibana, J. Reppert, A. Rao, T. Nishio, Y. Hasegawa, H. Sano, and Y. Iye, Appl. Phys. Lett. **95**, 142503 (2009).
[20] K.-P. Bohnen, R. Heid, and B. Renker, Phys. Rev. Lett. **86**, 5771 (2001).
[21] H. Hyodo, S. Araake, S. Hosoi, K. Soga, Y. Sato, M. Terauchi, and K. Kimura, Phys. Rev. B **77**, 024515 (2008).
[22] M. I. Eremets, V. V. Struzhkin, H.-k. Mao, and R. J. Hemley, Science **293**, 272 (2001).
[23] D. A. Papaconstantopoulos and M. J. Mehl, Phys. Rev. B **65**, 172510 (2002).
[24] K. Takei, K. Nakamura, and Y. Maeda, J. Appl. Phys. **57**, 5093 (1985).
[25] T. Zhang, P. Cheng, W.-J. Li, Y.-J. Sun, G. Wang, X.-G. Zhu, K. He, L. Wang, X. Ma, X. Chen *et al.*, Nat. Phys. **6**, 104 (2010).
[26] C. Si, Z. Liu, W. Duan, and F. Liu, Phys. Rev. Lett. **111**, 196802 (2013).
[27] I. Boustani, Phys. Rev. B **55**, 16426 (1997).
[28] H. Tang and S. Ismail-Beigi, Phys. Rev. Lett. **99**, 115501 (2007).
[29] X. Yang, Y. Ding, and J. Ni, Phys. Rev. B **77**, 041402 (2008).
[30] H. Tang and S. Ismail-Beigi, Phys. Rev. B **80**, 134113 (2009).
[31] H. Tang and S. Ismail-Beigi, Phys. Rev. B **82**, 115412 (2010).
[32] J. Kunstmann and A. Quandt, Phys. Rev. B **74**, 035413 (2006).
[33] M. H. Evans, J. D. Joannopoulos, and S. T. Pantelides, Phys. Rev. B **72**, 045434 (2005).
[34] X. Wu, J. Dai, Y. Zhao, Z. Zhuo, J. Yang, and X. C. Zeng, ACS Nano **6**, 7443 (2012).
[35] E. S. Penev, S. Bhowmick, A. Sadrzadeh, and B. I. Yakobson, Nano Lett. **12**, 2441 (2012).
[36] X. Yu, L. Li, X.-W. Xu, and C.-C. Tang, J. Phys. Chem. C **116**, 20075 (2012).
[37] K. C. Lau and R. Pandey, J. Phys. Chem. C **111**, 2906 (2007).
[38] X.-F. Zhou, X. Dong, A. R. Oganov, Q. Zhu, Y. Tian, and H.-T. Wang, Phys. Rev. Lett. **112**, 085502 (2014).
[39] H. Dekura, K. Shirai, and H. Katayama-Yoshida, J. Phys.: Condens. Matter **19**, 365241 (2007).
[40] A. R. Oganov and C. W. Glass, J. Chem. Phys. **124**, 244704 (2006).
[41] C. W. Glass, A. R. Oganov, and N. Hansen, Comput. Phys. Commun. **175**, 713 (2006).
[42] Q. Zhu, L. Li, A. R. Oganov, and P. B. Allen, Phys. Rev. B **87**, 195317 (2013).
[43] G. Kresse and J. Furthmüller, Phys. Rev. B **54**, 11169 (1996).
[44] G. Kresse and J. Furthmüller, Comput. Mater. Sci. **6**, 15 (1996).
[45] F. Liu, C. Shen, Z. Su, X. Ding, S. Deng, J. Chen, N. Xu, and H. Gao, J. Mater. Chem. **20**, 2197 (2010).
[46] J. P. Perdew, K. Burke, and M. Ernzerhof, Phys. Rev. Lett. **77**, 3865 (1996).
[47] J. Heyd, G. E. Scuseria, and M. Ernzerhof, J. Chem. Phys. **118**, 8207 (2003).
[48] P. Giannozzi, S. Baroni, N. Bonini, M. Calandra, R. Car, C. Cavazzoni, D. Ceresoli, G. L. Chiarotti, M. Cococcioni, I. Dabo *et al.*, J. Phys.: Condens. Matter **21**, 395502 (2009).
[49] G. Profeta, M. Calandra, and F. Mauri, Nat. Phys. **8**, 131 (2012).
[50] See Supplemental Material at http://link.aps.org/supplemental/10.1103/PhysRevB.93.014502 for the convergence testing, and additional structural, electronic, and vibrational properties of 2D boron allotropes.
[51] See AFLOW datebase at http://aflowlib.org/material.php?id=aflow:dd20fb91c03ac8d2.
[52] P. B. Allen and R. C. Dynes, Phys. Rev. B **12**, 905 (1975).
[53] S. L. Bud'ko, G. Lapertot, C. Petrovic, C. E. Cunningham, N. Anderson, and P. C. Canfield, Phys. Rev. Lett. **86**, 1877 (2001).